LETTERS
https://doi.org/10.1038/s41565-021-00987-0

nature nanotechnology

Check for updates

# Subambient daytime radiative cooling textile based on nanoprocessed silk

Bin Zhu[1,5], Wei Li[2,5], Qian Zhang[1,3], Duo Li[1], Xin Liu[1], Yuxi Wang[1], Ning Xu[1], Zhen Wu[1], Jinlei Li[1], Xiuqiang Li[1], Peter B. Catrysse[4], Weilin Xu[3], Shanhui Fan[4] ✉ and Jia Zhu[1] ✉

**Decreasing energy consumption is critical to sustainable development. Because temperature regulation for human comfort consumes vast amounts of energy, substantial research efforts are currently directed towards developing passive personal thermal management techniques that cool the human body without any energy consumption[1–9]. Although various cooling textile designs have been proposed previously, textile-based daytime radiative cooling to a temperature below ambient has not been realized[6–13]. Silk, a natural protein fabric produced by moth caterpillars, is famous for its shimmering appearance and its cooling and comforting sensation on skin[14–17]. It has been recently recognized that silk, with its optical properties derived from its hierarchical microstructure, may represent a promising starting point for exploring daytime radiative cooling[18–21]. However, the intrinsic absorption of protein in the ultraviolet region prevents natural silk from achieving net cooling under sunlight. Here we explore the nanoprocessing of silk through a molecular bonding design and scalable coupling reagent-assisted dip-coating method, and demonstrate that nanoprocessed silk can achieve subambient daytime radiative cooling. Under direct sunlight (peak solar irradiance > 900 W m$^{-2}$) we observed a temperature of ~3.5 °C below ambient (for an ambient temperature of ~35 °C) for stand-alone nanoprocessed silks. We also observed a temperature reduction of 8 °C for a simulated skin when coated with nanoprocessed silk, compared with natural silk. This subambient daytime radiative cooling of nanoprocessed silk was achieved without compromising its wearability and comfort. This strategy of tailoring natural fabrics through scalable nanoprocessing techniques opens up new pathways to realizing thermoregulatory materials and provides an innovative way to sustainable energy.**

As cooling accounts for ~15% of electricity use in the world, it is important to develop a passive personal thermal management strategy for human sustainable energy-saving development[1]. Throughout the long history of civilization, various fabrics and textiles have been used to bring comfort and glamour to the human body, as well as to protect it from temperature variations[2–4]. Recently, there are emerging efforts to design textiles with artificial structures to achieve radiative cooling effects for personal thermal management[5–9]. Most of these studies have focused on enhancing human body heat dissipation to the ambient environment through infrared-transparent textiles. As the ambient environment is the heat sink, it thermodynamically prohibits these types of textiles from realizing subambient cooling. In an outdoor situation, the sky (temperature 3 K) represents a far better heat sink as compared with the ambient environment. Therefore, textiles with high infrared emissivity have the potential to achieve subambient temperature (see Supplementary Schematic 1 for comparison). A subambient temperature is desirable for textiles as this could provide an even cooler sensation to skin compared with when skin is directly exposed to ambient temperature. Although various subambient radiative cooling materials and structures, such as thin films[10,11], woods[12] and painting[13], have been demonstrated, up to now textiles that can achieve subambient radiative cooling under sunlight have not been realized, not to mention their wearability and comfort.

For centuries, silk has been one of the most favourable fabrics, with its excellent moisture transportation, lustre appearance and cooling sensation[14–17]. The optical properties of silk are fundamentally related to its hierarchical structure, derived from the self-assembly of fibroin protein inside the silkworm. This self-assembled hierarchical structure of silk induces reflectivity in the visible (VIS) and near-infrared (NIR) range of the solar spectrum (wavelength, $\lambda \approx 0.3$–$2.5\,\mu$m). Meanwhile, its main component of fibroin protein possesses high emissivity in the mid-infrared (MIR) spectrum ($\lambda \approx 8$–$13\,\mu$m) to minimize the thermal load[18–21] (Supplementary Figs. 1–3). Therefore, natural silk has been considered as a promising candidate for radiative cooling[20,21].

However, for silk to achieve subambient radiative cooling, it is important to consider the net cooling power from a heat balance analysis:

$$P_{\mathrm{cool}}(T) = P_{\mathrm{rad}}(T) - P_{\mathrm{atm}}(T_{\mathrm{amb}}) - P_{\mathrm{Sun}} - P_{\mathrm{cond+conv}} \quad (1)$$

where $P_{\mathrm{cool}}(T)$ is the net radiative cooling power in the absence of sunlight, $P_{\mathrm{rad}}(T)$ is the power radiated out through the atmospheric transmission window, $P_{\mathrm{atm}}(T_{\mathrm{amb}})$ is the absorbed power due to incident atmospheric thermal radiation, $P_{\mathrm{Sun}}$ corresponds to the incident solar power absorbed and $P_{\mathrm{cond+conv}}$ is the power lost due to convection and conduction. It is clear that even for a material with ideal selective thermal emission only in the atmospheric transparency window, over 90% of incident sunlight still must be reflected to achieve subambient temperature[10].

[1]National Laboratory of Solid State Microstructures, College of Engineering and Applied Sciences, Jiangsu Key Laboratory of Artificial Functional Materials, Frontiers Science Center for Critical Earth Material Cycling, Nanjing University, Nanjing, People's Republic of China. [2]GPL Photonics Lab, State Key Laboratory of Applied Optics, Changchun Institute of Optics, Fine Mechanics and Physics, Chinese Academy of Sciences, Changchun, People's Republic of China. [3]State Key Laboratory of New Textile Materials and Advanced Processing Technologies, School of Textile Science and Engineering, Wuhan Textile University, Wuhan, People's Republic of China. [4]Department of Electrical Engineering, Ginzton Laboratory, Stanford University, Stanford, CA, USA. [5]These authors contributed equally: Bin Zhu, Wei Li. ✉e-mail: shanhui@stanford.edu; jiazhu@nju.edu.cn

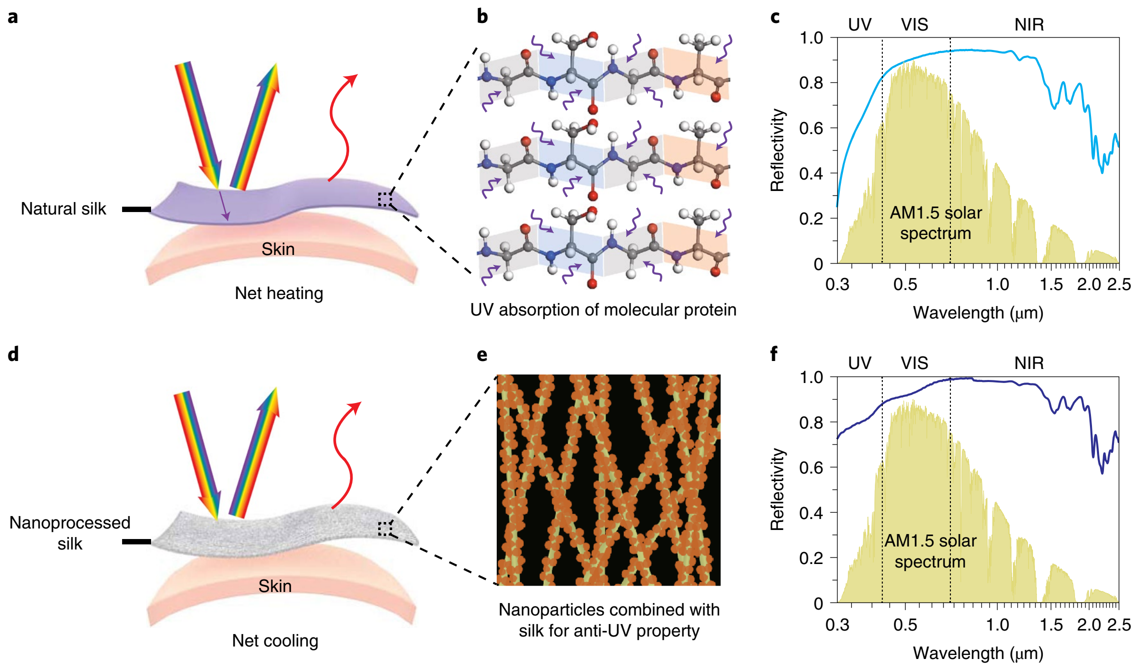


**Fig. 1 | Subambient daytime radiative cooling design for nanoprocessed silk. a**, Schematic of the net heating performance of natural silk due to the high absorption in the UV region. **b**, Schematic of the UV absorption by the protein molecule of silk. **c**, The reflectivity spectrum of natural silk in the 0.3–2.5 μm wavelength range. The overall reflectivity in the sunlight wavelength range is about 86%. **d**, Schematic of the net cooling performance of nanoprocessed silk by enhancing UV reflectance. **e**, Schematic of nanoprocessed silk with enhanced anti-UV property, achieved by connecting nanoparticles to silk through a coupling reagent. **f**, The reflectivity spectrum of nanoprocessed silk in the 0.3–2.5 μm wavelength range. The overall reflectivity in the sunlight wavelength range is about 95%.

Natural silk intrinsically shows high absorption in the ultraviolet (UV) region[22] due to its protein component (Fig. 1a,b). Consequently, its overall reflectivity in the sunlight wavelength range (0.3–2.5 μm) is only ~86% (Fig. 1c), which fundamentally prohibits it from achieving a net cooling power or subambient temperature under sunlight in the daytime.

Therefore, to develop silk-based fabrics for subambient daytime radiative cooling, it would be desirable to develop processes that increase the reflectivity of silk in the UV wavelength range without negatively affecting its thermal emission properties. Moreover, the processing needs to preserve its excellent wearability. For these reasons then, first, the process should not destroy the inherent hierarchical structure and unique components of silk, which are fundamentally related to its optical properties (Supplementary Figs. 1–3). Second, properties such as moisture transportation and air permeability are essential to the comfort of fabrics and therefore should not be sacrificed. In addition, the subambient daytime radiative cooling properties after treatment need to be durable, even after wearing, twisting and washing. Also, the treatment process should be scalable and compatible with large-scale fabric manufacturing techniques.

To meet these requirements, here we processed silk through a scalable coupling reagent-assisted dip-coating method, and demonstrate positive net cooling power under sunlight (Fig. 1d). We also show that such nanoprocessing preserves the wearability of silk. To enhance the reflectivity in the UV wavelength region, we bonded inorganic oxide nanoparticles, which have a high refractive index, to silk through a molecular bonding strategy using a coupling reagent (Fig. 1e). Both theoretical simulations and experimental results confirmed that these nanoparticles increase the reflectivity of silk from 70 to 85% in the UV range (300–420 nm). In addition, the reflectivity in the VIS-NIR range is also enhanced, and the overall reflectivity of silk can reach approximately 95% across the full solar spectrum (Fig. 1f). Therefore, combined with the intrinsic high emissivity of silk in the wavelength range of 8–13 μm, the nanoprocessed silk experimentally realizes a subambient temperature drop of ~3.5 °C in the daytime. Furthermore, the silk fabric, after this coupling reagent-assisted dip-coating process, preserves excellent moisture transportation and durability. We have therefore demonstrated a promising high-performance, wearable material for personal thermal management, together with a nanoprocessing method that is amenable to large-scale practical production.

Various metal oxide materials have been used to block UV light due to their UV absorption properties, for example, titanium oxide[23–26]. However, to realize subambient cooling performance, such UV absorption materials cannot be used here to avoid thermal load. Aluminium oxide has a high refractive index ($n \approx 1.8$) and shows minimum absorption in the UV region[27]. Thus, it was expected that $Al_2O_3$ nanoparticles could be used to increase the UV reflectivity of silk. The reflectivity of nanoparticles is strongly dependent on their size. We therefore calculated the scattering efficiency of $Al_2O_3$ particles as a function of particle size across the UV spectrum using Mie scattering theory[28]. As shown in Fig. 2a, strong scattering in the UV wavelength range can be achieved for particle sizes between 250 and 350 nm. On the other hand, in the MIR wavelength range, which is important for thermal emission, incorporating such nanoparticles into silk does not affect the low reflectivity and high emissivity of silk, because the particle sizes are much smaller than the thermal wavelength. Therefore, $Al_2O_3$ nanoparticles with a size of approximately 300 nm were used in the subsequent experiments (Supplementary Fig. 4).

The next step was to adhere the $Al_2O_3$ particles to the silk without affecting the other properties of silk. Dip coating, as a low-cost, high-throughput and scalable technique, has been widely applied to functionalize fibres[29,30]. However, it has rarely been used to functionalize natural silks[29] because it is challenging to adhere

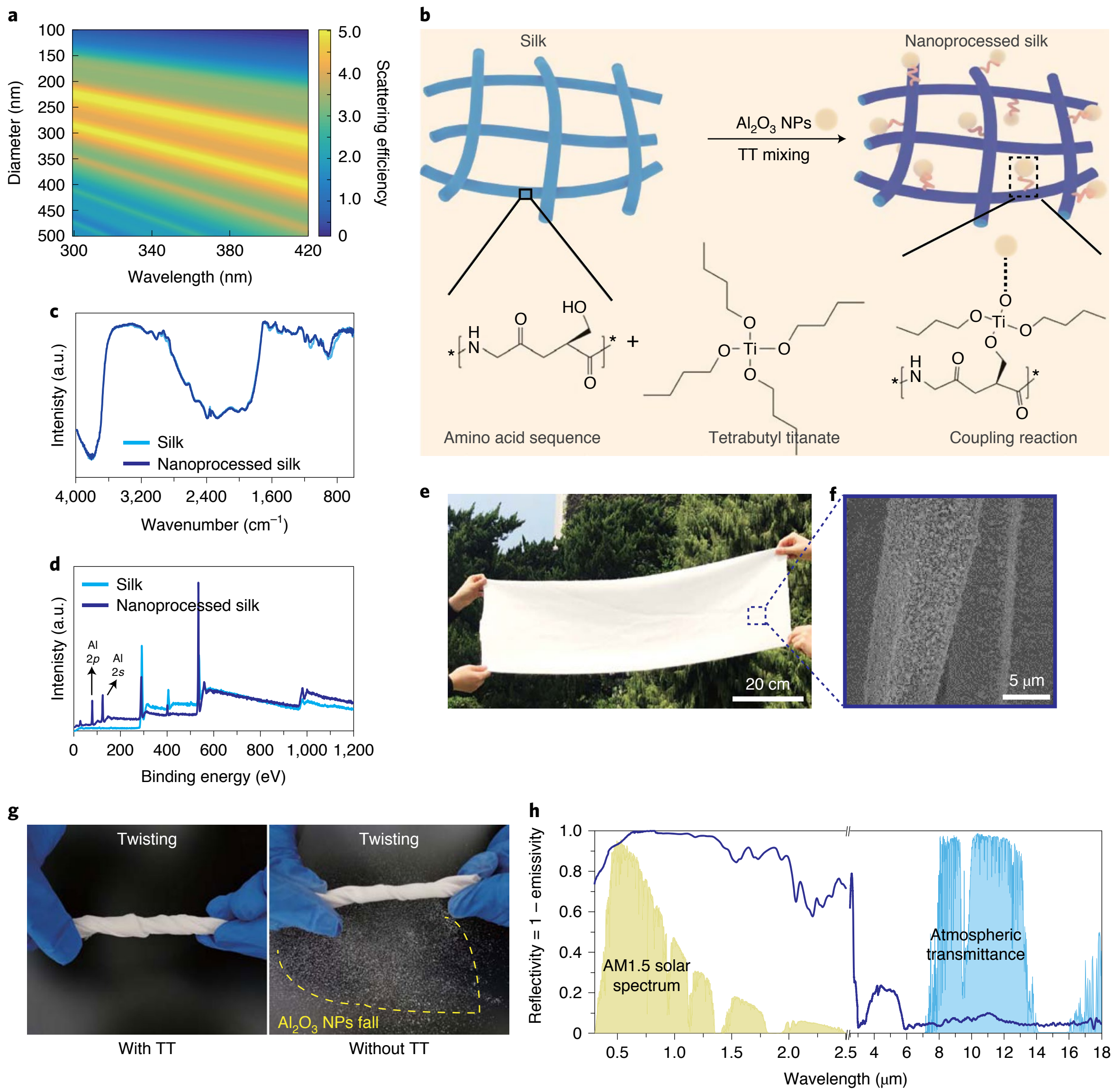


**Fig. 2 | Preparation and characterization of nanoprocessed silk. a**, Simulation of the normalized scattering efficiency of $Al_2O_3$ particles in silk over the wavelength range of 0.3–0.42 μm, with the particle diameter varying from 0.1 to 0.5 μm. **b**, Schematic for the fabrication of nanoprocessed silk. Tetrabutyl titanate was used as a coupling reagent to facilitate the bonding of $Al_2O_3$ nanoparticles (NPs) to silk fibres through a coupling reaction. The asterisks represent other amino acid structures omitted for clarity. **c**,**d**, FTIR (**c**) and XPS (**d**) spectra of natural silk and nanoprocessed silk. **e**, Photograph of the nanoprocessed silk fabric. **f**, High-magnification SEM image of an individual nanoprocessed silk yarn with the $Al_2O_3$ particles clearly visible. **g**, Optical images of nanoprocessed silk fabric with and without TT treatment after stretching and twisting. None of the $Al_2O_3$ nanoparticles fell onto the table after TT treatment due to the induced adhesion, contrary to observations without TT treatment. **h**, The reflectivity spectrum of nanoprocessed silk in the 0.3–18 μm wavelength range.

functional components onto natural fibres without destroying their structure and properties. Inspired by the coupling reaction used in plasthetics[31], tetrabutyl titanate (TT) was chosen as coupling reagent to connect the $Al_2O_3$ particles to silk (see the Methods and Supplementary Information for details). TT can form hydrogen bonds with the hydroxy groups on the surface of $Al_2O_3$ and also reduces the agglomeration of $Al_2O_3$ particles. At the same time, TT can form strong covalent bonds with the amino acids of silk. Therefore, strong bonds and good adhesion between $Al_2O_3$ particles and silk are formed through this molecular bonding design strategy (Fig. 2b). Analysis by Fourier-transform infrared (FTIR) and X-ray photoelectron spectroscopy (XPS) confirmed that the components of silk fibre remained unchanged upon coupling with $Al_2O_3$ particles (Fig. 2c,d).

Figure 2e shows a piece of woven silk fabric after nanoprocessing (Supplementary Fig. 5). The scanning electron microscopy (SEM) images in Fig. 2f and Supplementary Fig. 6 clearly show the uniform distribution of $Al_2O_3$ nanoparticles on the silk. To verify the adherence of the $Al_2O_3$ nanoparticles to the silk fibre, the nanoprocessed silk fabric was deformed by stretching, flexing and twisting (Fig. 2g, Supplementary Fig. 7 and Supplementary Video 1). None of the $Al_2O_3$ nanoparticles fell off the silk when the fabric was flexed and twisted. It was also found that the reflectivity of the nanoprocessed silk after 1,000 dynamic twisting cycles was similar to that of the original sample (Supplementary Fig. 8 and Video 2). As a comparison, we also tried to incorporate $Al_2O_3$ particles directly into silk without the TT additive; in this case, large amounts of $Al_2O_3$ nanoparticles were observed to detach when the silk fabric was

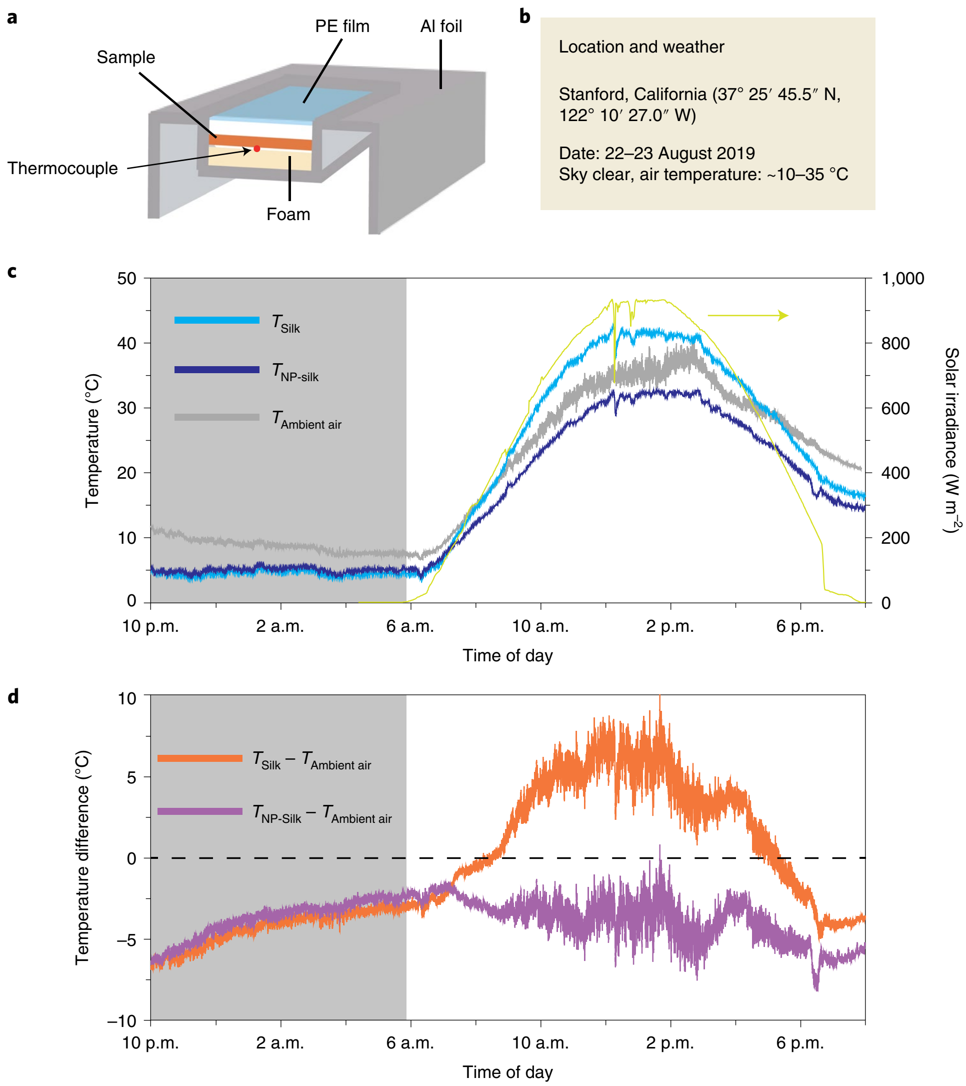


**Fig. 3 | Measurement of the radiative cooling performance of natural and nanoprocessed silk. a**, Schematic of the radiative cooling set-up used to measure the radiative cooling performance of the silk fabrics in Stanford, California. **b**, Topographic and meteorological information of the test location. **c**, The temperature data measured for natural silk, nanoprocessed silk (NP-silk) and ambient air, along with the solar irradiance. After nanoprocessing, the nanoprocessed silk presents obviously lower temperatures than the ambient air during the daytime, whereas the temperature of pristine silk is higher than the air temperature. **d**, The temperature difference between ambient air and natural silk, and between ambient air and nanoprocessed silk.

deformed (Fig. 2g and Supplementary Video 3). Therefore, the addition of TT is essential for increasing the adhesion between the $Al_2O_3$ nanoparticles and silk, and for ensuring good durability while wearing the nanoprocessed silk. The reflectivity spectrum of nanoprocessed silk in Fig. 2h shows high reflectivity of approximately 0.95 in the solar light region and high emissivity of ~0.9 in the 8–13 µm wavelength range. In addition, the solar reflectivity and infrared emissivity spectral responses show negligible angular dependence (Supplementary Fig. 9), thereby suggesting the potential of this material for excellent subambient radiative cooling performance.

We performed continuous radiative cooling measurements for 22 h on both natural silk and nanoprocessed silk on a clear day in Stanford, California (37° 25′ 45.5″ N, 122° 10′ 27.0″ W). Samples of nanoprocessed silk and natural silk were placed side by side in two similar enclosures, and the temperatures of the samples were measured simultaneously, along with the air temperature and the solar irradiance (Fig. 3a,b). Although the temperature of natural silk was lower than the ambient temperature during the night time due to its thermal emission, in the daytime (9 a.m. to 5 p.m.) under sunlight its temperature was usually above ambient due to solar heating (Fig. 3c). In contrast, the temperature of the nanoprocessed silk was consistently below the ambient temperature during both the day and night. Even during the time period of 11 a.m. to 3 p.m., when the solar irradiance was over 800 W m$^{-2}$, the nanoprocessed silk still showed on average a temperature approximately 3.5 °C below the ambient air temperature (Fig. 3d). The results here clearly illustrate the importance of nanoprocessing for achieving subambient daytime radiative cooling with silk.

We also examined the cooling performance of silk when it was used to cover a simulated skin placed under sunlight in Stanford, California (Fig. 4a; see Supplementary Table 1 for detailed weather information). The simulated skin comprised a silicone rubber insulated flexible heater. With a constant input power, the skin temperature was determined by how the heat was dissipated (Fig. 4b). When covered with nanoprocessed silk, the skin had a temperature that was ~8, ~12.5 and ~19 °C lower than the same skin covered with natural silk or cotton, or left uncovered, respectively (Fig. 4c,d). It is noteworthy that the three different textiles all showed

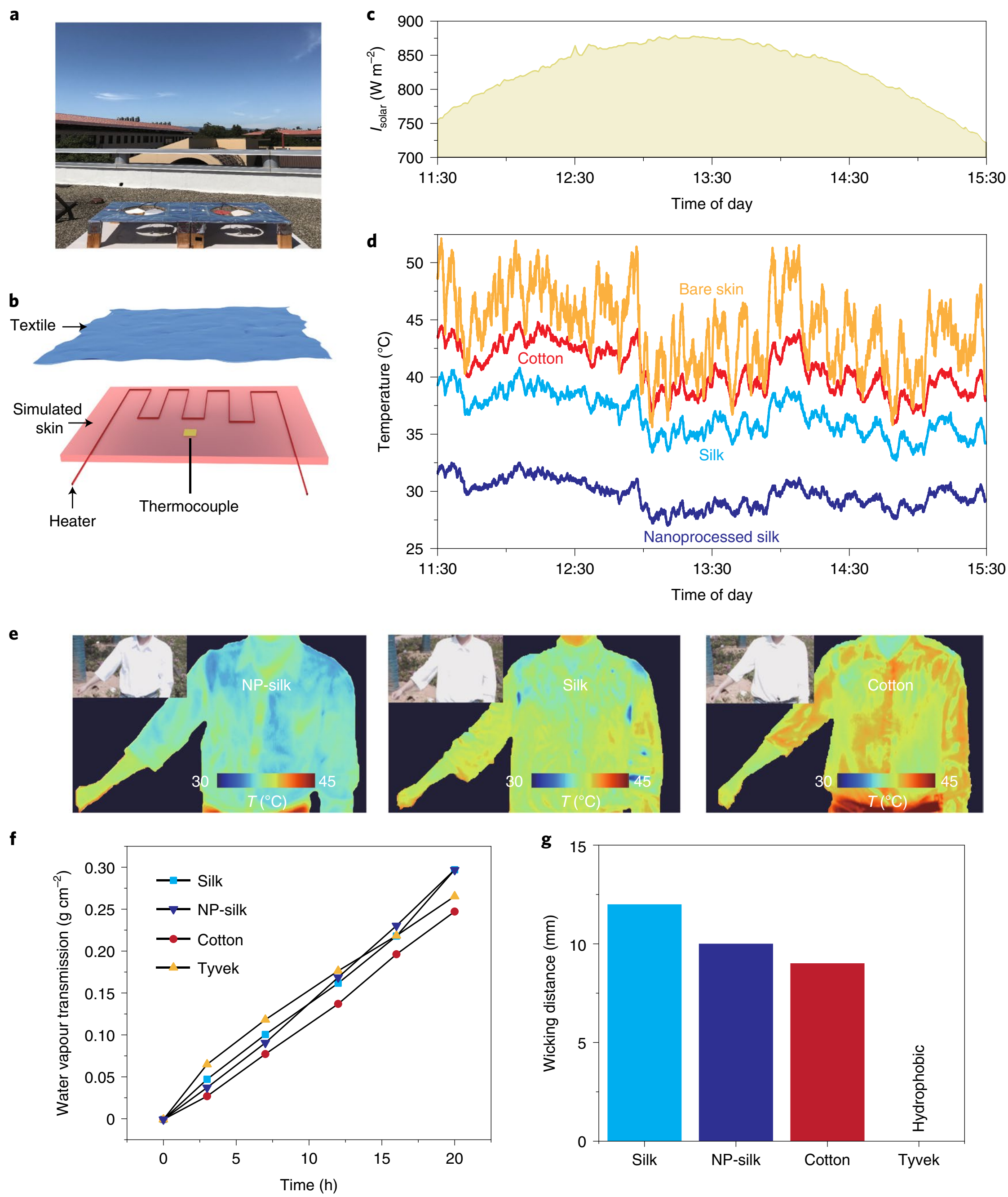


**Fig. 4 | Thermal measurement of wearing nanoprocessed silk and its wearable performance.** **a**, Photograph of the set-up used for the thermal measurement of simulated skin under sunlight in Stanford, California. **b**, Schematic of the set-up, which consists of a heater increasing the temperature to simulate human skin, a thermocouple measuring the simulated skin temperature and a textile sample covering the simulated skin. **c**,**d**, Solar irradiance ($I_{solar}$; **c**) and temperature data (**d**) for the bare simulated skin and the simulated skin covered with cotton, silk or nanoprocessed silk over a duration of 4 h under sunlight in Stanford, California. The simulated skin covered with nanoprocessed silk presents obviously lower temperatures than silk-covered, cotton-covered and bare skin. **e**, Infrared images and optical photographs (insets) of a human wearing shirts made from nanoprocessed silk, silk and cotton under sunlight in Nanjing. The temperature of the nanoprocessed silk shirt is lower than that of the silk and cotton shirts at the ambient temperature of 37 °C. The background temperature from buildings has been subtracted for clearance. **f**, Water vapour transmission rates of different textiles measured over time. Even after treatment, nanoprocessed silk still presents good transmission of water vapour from human perspiration. **g**, Wicking distance of different textiles, showing their ability to transport perspiration for quick evaporation.

a similarly low transmittance (Supplementary Fig. 10). Figure 4e presents the infrared images of a human wearing garments made of the three different textiles under a clear sky in Nanjing, China (see Supplementary Table 1 for detailed topographic and meteorological information), with the ambient temperature around 37 °C. The images show that the outer surface temperature of the nanoprocessed silk is lower than those of natural silk and cotton. Therefore, it will provide a cooler sensation. Taking into account the thermal conducting properties of the textiles, the lower temperature of the nanoprocessed silk can be directly attributed to its radiative cooling capability (Supplementary Table 2 and Supplementary Fig. 11). All the results above illustrate the superior cooling ability of nanoprocessed silk, due to the combination of its enhanced solar reflection (especially its anti-UV property), which minimizes heat input, as well as its inherent thermal radiation properties, which are unaffected by nanoprocessing.

In addition to its radiative cooling properties, it was also important to examine other metrics of the nanoprocessed silk related to human comfort. For this purpose, cotton and Tyvek, which is a widely used commercial fibrous polyethylene (PE) textile, were used for comparison. The water vapour transmission rate (WVTR) reflects the ability of a fabric to transmit water vapour from perspiration through natural diffusion and convection. The nanoprocessed silk presented a similar WVTR to natural silk and Tyvek, which was slightly higher than that of cotton (Fig. 4f). The wicking rate is a measure of the transport of liquid water in textiles, with a higher wicking rate corresponding to a higher rate of perspiration spread and evaporation. Among all of the natural textiles, silk shows the highest wicking rate because of its good hydrophilicity. With a coating of $Al_2O_3$ nanoparticles, silk still has a wicking distance of 10 mm, which is comparable to that of natural silk (Fig. 4g). As a comparison, Tyvek is hydrophobic and therefore does not have any wicking length. The nanoprocessed silk also maintains good air permeability after $Al_2O_3$ processing (Supplementary Fig. 12). All of these results show that silk fabric retains good wearability with a coating of $Al_2O_3$ nanoparticles. The washability of the nanoprocessed silk fabric was also tested by water washing and sunlight drying. After a regular duration of washing and drying, the nanoprocessed silk fabric was unchanged (Supplementary Figs. 13 and 14). Through careful examination, it was found that after several washing–drying cycles, the $Al_2O_3$ nanoparticles remained well-adhered to the silk, and the nanoprocessed silk maintained satisfactory UV reflectivity (Supplementary Fig. 15). Therefore, we have demonstrated that the nanoprocessed silk fabric is durable through washing and drying. In addition to maintaining the cool-to-touch feature of silk, which is one of its favourite properties, we also applied the screen printing technique to coat $Al_2O_3$ nanoparticles only on the outer side of silk that faces the sunlight, while the skin is in direct contact with the inner side of natural silk (Supplementary Video 4). The obtained samples endured 50 cycles of accelerated washing and drying (Supplementary Video 5 and Supplementary Fig. 16). We note that nanoparticles have been used in textile and cosmetic industries. Although the fall-off of nanoparticles after many washing cycles may cause potential environmental and health hazards[32], it is expected that various strategies, such as the development of binders and the conformal coating technique, which enhances the connection between nanoparticles and textiles, could be used to address these issues.

In summary, the strong absorption of natural silk in the UV wavelength region prevents it from achieving subambient radiative cooling performance. We have demonstrated that through a molecular bonding design strategy and scalable dip-coating methods, nanoprocessed silk can achieve a temperature of ~3.5 °C below ambient in the daytime, and when covering simulated skin can achieve a reduction of skin temperature of ~8 °C under sunlight, with similar comfort and wearability to natural silk. The subambient radiative cooling effect achieved under sunlight means that skin will achieve the same cooling sensation in contact with this nanoprocessed silk, if not better, when skin is directly exposed to ambient temperature. We anticipate that this strategy of tailoring natural materials through convenient and scalable processes may not only provide a sustainable energy-saving approach to personal thermal management, but also inspire new pathways for the development of materials and devices for passive cooling to reduce energy consumption.

## Online content

Any methods, additional references, Nature Research reporting summaries, source data, extended data, supplementary information, acknowledgements, peer review information; details of author contributions and competing interests; and statements of data and code availability are available at https://doi.org/10.1038/s41565-021-00987-0.

Received: 5 February 2021; Accepted: 31 August 2021;
Published online: 8 November 2021

## References

1. Office of Energy Saver. Heating and Cooling *US Department of Energy* www.energy.gov/heating-cooling
2. Rödel, H., Schenk, A., Herzberg, C. & Krzywinski, S. Links between design, pattern development and fabric behaviours for clothes and technical textiles. *Int. J. Cloth. Sci. Tech.* **13**, 217–227 (2001).
3. Cho, S. C. et al. Surface modification of polyimide films, filter papers, and cotton clothes by HMDSO/toluene plasma at low pressure and its wettability. *Curr. Appl. Phys.* **9**, 1223–1226 (2009).
4. Parvari, R. A. et al. The effect of fabric type of common Iranian working clothes on the induced cardiac and physiological strain under heat stress. *Arch. Environ. Occup. Health* **70**, 272–278 (2015).
5. Hsu, P. C. et al. Radiative human body cooling by nanoporous polyethylene textile. *Science* **353**, 1019–1023 (2016).
6. Peng, Y. et al. Nanoporous polyethylene microfibres for large-scale radiative cooling fabric. *Nat. Sustain.* **1**, 105–112 (2018).
7. Zhang, X. et al. Dynamic gating of infrared radiation in a textile. *Science* **363**, 619–623 (2019).
8. Cai, L. et al. Spectrally selective nanocomposite textile for outdoor personal cooling. *Adv. Mater.* **30**, 1802152 (2018).
9. Hsu, P. C. et al. A dual-mode textile for human body radiative heating and cooling. *Sci. Adv.* **3**, e1700895 (2017).
10. Raman, A. P., Anoma, M. A., Zhu, L., Rephaeli, E. & Fan, S. Passive radiative cooling below ambient air temperature under direct sunlight. *Nature* **515**, 540–544 (2014).
11. Zhai, Y. et al. Scalable-manufactured randomized glass-polymer hybrid metamaterial for daytime radiative cooling. *Science* **355**, 1062–1066 (2017).
12. Li, T. et al. A radiative cooling structural material. *Science* **364**, 760–763 (2019).
13. Mandal, J. et al. Hierarchically porous polymer coatings for highly efficient passive daytime radiative cooling. *Science* **362**, 315–319 (2018).
14. Yang, Y. & Li, S. Silk fabric non-formaldehyde crease-resistant finishing using citric acid. *J. Text. Inst.* **84**, 638–644 (1993).
15. Gong, R. H. & Mukhopadhyay, S. K. Fabric objective measurement: a comparative study of fabric characteristics. *J. Text. Inst.* **84**, 192–198 (1993).
16. Huang, F., Wei, Q., Liu, Y., Gao, W. & Huang, Y. Surface functionalization of silk fabric by PTFE sputter coating. *J. Mater. Sci.* **42**, 8025–8028 (2007).
17. Cai, Z., Jiang, G. & Yang, S. Chemical finishing of silk fabric. *Color. Technol.* **117**, 161–165 (2001).
18. Shi, N. et al. Keeping cool: enhanced optical reflection and heat dissipation in silver ants. *Science* **349**, 298–301 (2015).
19. Jin, H. & Kaplan, D. L. Mechanism of silk processing in insects and spiders. *Nature* **424**, 1057–1061 (2003).
20. Choi, S. et al. Anderson light localization in biological nanostructures of native silk. *Nat. Commun.* **9**, 452 (2018).
21. Shi, N. et al. Nanostructured fibers as a versatile photonic platform: radiative cooling and waveguiding through transverse Anderson localization. *Light Sci. Appl.* **7**, 37 (2018).
22. Rosenheck, K. & Doty, P. The far ultraviolet absorption spectra of polypeptide and protein solutions and their dependence on conformation. *Proc. Natl Acad. Sci. USA* **47**, 1775–1785 (1961).
23. Yang, H., Zhu, S. & Pan, N. Studying the mechanisms of titanium dioxide as ultraviolet-blocking additive for films and fabrics by an improved scheme. *J. Appl. Polym. Sci.* **92**, 3201–3210 (2004).
24. Wang, J., Tsuzuki, T., Sun, L. & Wang, X. Reverse microemulsion-mediated synthesis of $SiO_2$-coated ZnO composite nanoparticles: multiple cores with tunable shell thickness. *ACS Appl. Mater. Interfaces* **2**, 957–960 (2010).
25. Fan, J. & Hunter, L. *Engineering Apparel Fabrics and Garments* (Woodhead Publishing, 2009).
26. Yusuf, M. A review on flame retardant textile finishing: current and future trends. *Curr. Smart Mater.* **3**, 99–108 (2018).
27. Patil, P. V., Bendale, D. M., Puri, R. K. & Puri, V. Refractive index and adhesion of $Al_2O_3$ thin films obtained from different processes—a comparative study. *Thin Solid Films* **288**, 120–124 (1996).
28. Mie, G. Beiträge zur Optik trüber Medien, speziell kolloidaler Metallösungen. *Ann. Phys.* **330**, 377–445 (1908).

29. Steven, E. et al. Carbon nanotubes on a spider silk scaffold. *Nat. Commun.* **4**, 2435 (2013).
30. Zhang, W. et al. Tensan silk-inspired hierarchical fibers for smart textile applications. *ACS Nano* **12**, 6968–6977 (2018).
31. Corbet, J. & Mignani, G. Selected patented cross-coupling reaction technologies. *Chem. Rev.* **106**, 2651–2710 (2006).
32. Riaz, S. et al. Functional finishing and coloration of textiles with nanomaterials. *Color. Technol.* **134**, 327–346 (2018).

## Methods

**Preparation of a regenerated silk film for refractive index test.** For the refractive index test, we prepared regenerated silk films following a previously reported method[33]. After degumming silkworm cocoons, we removed the silk and then spread it over a clean piece of aluminium foil. We then dried the silk fibroin in a fume hood overnight. The regenerated silk films were then prepared as follows:

(1) Dissolving silk fibroin in LiBr. First we added LiBr to water to prepare 9.3 M LiBr solution. Then we packed the silk fibroin tightly into a 10-ml glass beaker and added the required amount of LiBr solution on top. The whole dissolvation of fibroin was processed in an oil bath pan at 60 °C. The solution turned amber in colour and transparent once the silk fibroin had completely dissolved.
(2) Dialysis and centrifugation. We added the silk–LiBr solution to a 3–12 ml dialysis bag (3,500 molecular weight cut-off; Shanghai Yuanye Bio-Technology). The solution was dialysed against 500 ml deionized water per 10 ml cassette. After dialysis we placed the silk–LiBr solution in a 40-ml centrifuge tube for centrifugation. After centrifugation to remove impurities, we transferred the silk solution into a culture dish.
(3) Silk film preparation. First, we added 4 ml of an 8% (wt/vol) aqueous silk solution to a 100-mm Petri dish. Films were generally produced with a thickness of 50 µm and could be easily removed from the polystyrene dish. For thicker films, we either increased the amount of silk solution or the concentration of silk, and then dried them. We filled the bottom of a vacuum desiccator with water and placed the dry films in the desiccator under vacuum. Finally, we gently removed the regenerated silk films from the dish.

**$Al_2O_3$ nanoparticle-treated silk fabric.** The silk fabric was commercially available and bought online (Saint Joy). Then we cut the fabric into pieces of the appropriate size for experiments. $Al_2O_3$ nanoparticles incorporated into the silk fabric can improve its optical reflectivity in the UV range. $Al_2O_3$ nanopowders (Macklin) were first dissolved in deionized water at a mass concentration of 18 g l$^{-1}$. We then added TT at a mass concentration of 12 g l$^{-1}$ to obtain a nano-$Al_2O_3$ hydrosol after ultrasonic dispersion for 20 min. Next, several pieces of silk fabric were immersed in a fatty alcohol polyoxyethylene ether solution (1 wt%) at 30 °C to clean the surface of the silk and then dried in an oven at 60 °C. The treated pieces of silk were dipped in the nano-$Al_2O_3$ hydrosol at 40 °C in a water bath heater and subsequently dried in an oven at 80 °C. The samples were stirred in deionized water to remove any nanoparticles on the surfaces of the samples. Finally, the clean samples were dried at room temperature.

**Reflectivity measurement.** The optical reflectance spectra of the silk and nanoprocessed silk fabrics were recorded separately in the UV to NIR (0.3–2.5 µm) and MIR (2.5–18 µm) wavelength ranges. In the first range, spectra were recorded with a UV-VIS-NIR spectrophotometer (UV 3600, Shimadzu) equipped with an integrating sphere model (ISR-3100, Shimadzu). For the second range, an FTIR spectrometer (Nicolet IS50, ThermoFisher) equipped with a gold integrating sphere (IntegatIR MIR, Pike) and a mercury cadmium telluride detector were used. Angular measurements were taken with the samples placed inside the integrating spheres at different angles to intercept the incident light.

**Refractive index measurement.** Refractive index measurements of the silk protein in the regenerated silk films were taken using a RC2 XI+ instrument (J.A. Woollam).

**Imaging.** Images of the silk and nanoprocessed silk fabric samples were taken using a Nikon camera (D7500). SEM was performed with a Zeiss Sigma VP scanning electron microscope. The infrared images were taken using a FLUKE Ti 100 infrared camera.

**Outdoor thermal measurements.** A silicone rubber insulated flexible heater (Omega, 39 cm$^2$) connected to a power supply (Keithley 2400) was used to simulate skin. The heating power density was 104 W m$^{-2}$. To avoid heat loss, an insulating foam was placed below the simulated skin heater. A ribbon-type hot thermocouple (K-type, Omega) was placed on the top surface of the heater to measure the temperature of the simulated skin. The textile sample was placed on the simulated skin, which we placed in an aluminized Mylar-coated wooden frame. A clear acrylic box with the top side open was joined to the underside of the wooden frame's top surface and sealed. A polystyrene pedestal covered with aluminized Mylar was glued to the acrylic box. The top opening of the wooden frame was left exposed to sunlight and air to mimic typical outdoor conditions in the presence of solar heating and convective airflow cooling. We measured and recorded the real-time temperatures of cotton-covered, nanoprocessed silk-covered, silk-covered and bare simulated skin, as well as the ambient temperature. The solar irradiance was recorded using a pyranometer (CMP 6, Kipp & Zonen). The simulated skin was removed to measure the daytime radiative cooling of pristine and nanoprocessed silk (Fig. 3c).

**Water vapour transmission rate test.** First, 40-ml bottles were filled with distilled water and sealed with the textile samples and rubber bands. The sealed bottles were then placed in an environmental chamber, where the temperature was maintained at 35 °C at a relative humidity of 40%. The bottles and samples were weighed continuously, and reductions in mass should arise from the evaporation of water. The reductions in mass were then divided by the area of the samples to obtain the water vapour transmission.

**Wicking test.** The textile samples were cut into 2-cm-wide strips and dipped in distilled water. The water started to climb up the samples by capillary force. The wicking test was performed for 60 s.

**Air permeability.** The different fabric samples were sealed between two pipes using flange adapters, a centring O-ring and a clamp. The exposed area of textile was 3 cm in diameter. One pipe was connected to a T-connector at the short/straight leg and then connected to the compressed air source. The other pipe was also connected to a T-connector at the short/straight leg and then connected to open air. A differential pressure gauge was connected to both long/branch legs to measure the pressure drops across the textile sample at different air flow rates.

**Thermal conductivity test.** The thermal conductivities, $\lambda$ (W K$^{-1}$ m$^{-1}$), of the three samples (NP-silk, silk and cotton) were calculated as $\lambda = \alpha \times C_p \times \rho$, where $\alpha$ is the thermal diffusivity (mm$^2$ s$^{-1}$), $C_p$ is the specific heat capacity (J g$^{-1}$ K$^{-1}$) and $\rho$ is the density (g cm$^{-3}$). The thermal diffusivities of the samples were measured using an LFA 467 Hyperflash instrument (NETZSCH), $C_p$ was measured under nitrogen atmosphere using a Pyris Diamond differential scanning calorimeter (Perkin-Elmer) and $\rho$ was determined by liquid displacement measurement.

**Screen printing.** $Al_2O_3$ powders were dispersed in a binder solution (Helizarin Binder UDT) with stirring. This homogeneous solution was transferred onto a screen with a fine mesh (~150 µm). The mixture was then deposited onto the silk fabric through the mesh by moving a squeegee across the screen. Finally, the nanoprocessed silk samples were obtained after drying.

**Washing test of the fabric.** The washing performance of the screen-printed nanoprocessed silk fabric was assessed according to the American Association of Textile Chemists and Colorists international standard (AATCC 61-2013). A standard washing machine (SW-LZA, Changzhou Dahua Electronic Instrument) was used in this study. The fabric samples were washed at 60 °C for 30 min in a rotating closed canister containing 200 g of water, 1 g of liquid detergent and 10 steel balls (6 mm in diameter). Then the fabrics were rinsed with water and dried at 70 °C.

**Fatigue twisting test.** The nanoprocessed silk was continuously twisted using a yarn twist machine (Y331C, Wuhan Guoheng Instrument).

## Data availability

All relevant data are included in the manuscript and Supplementary Information. More detailed protocols, calculations and analyses are available from the authors upon request.

## References

33. Rockwood, D. et al. Materials fabrication from *Bombyx mori* silk fibroin. *Nat. Protoc.* **6**, 1612–1631 (2011).

## Acknowledgements

We acknowledge the Micro-fabrication Center of the National Laboratory of Solid State Microstructures (NLSSM) for technical support. J.Z. acknowledges the support from the Xplorer Prize. This work was jointly supported by the National Key Research and Development Program of China (grant no. 2017YFA0205700), the National Natural Science Foundation of China (grant nos. 52002168, 12022403, 51925204, 11874211, 62134009, 62121005 and 61735008), the Science Foundation of Jiangsu (grant no. BK20190311), the Excellent Research Program of Nanjing University (grant no. ZYJH005), the research foundation of Frontiers Science Center for Critical Earth Material Cycling (grant no. JBGS2106) and the Fundamental Research Funds for the Central Universities (grant nos. 021314380184, 021314380208, 021314380190, 021314380140 and 021314380150). S.F. acknowledges the support of the US Department of Energy (grant no. DE-FG-07ER46426).

## Author contributions

B.Z., W.L., J.Z. and S.F. designed the experiments. B.Z., Q.Z., D.L., J.L., X.L., Y.W. and W.X. prepared and characterized the materials and also performed the human wearing measurements and analysis. B.Z., X.L., Z.W., J.L., X.L. and N.X. contributed to the optical and thermal measurements and analysis. W.L. performed the outdoor test in Stanford. W.L. and P.B.C. performed the calculations. B.Z., W.L., S.F. and J.Z. wrote the manuscript.

## Competing interests

The authors declare no competing interests.

## Additional information

**Supplementary information** The online version contains supplementary material available at https://doi.org/10.1038/s41565-021-00987-0.

**Correspondence and requests for materials** should be addressed to Shanhui Fan or Jia Zhu.

**Peer review information** *Nature Nanotechnology* thanks Liangbing Hu and the other, anonymous, reviewer(s) for their contribution to the peer review of this work.